JOURNAL OF SPACECRAFT AND ROCKETS
Vol. 41, No. 4, July–August 2004

Effect of Orbit Data Quality on the Feasibility of Collision Risk Management

Alan B. Jenkin*
The Aerospace Corporation, Los Angeles, California 90009-2957

An analysis was performed to determine the effect of orbit data quality on the feasibility of collision risk management in low Earth orbit. Collision risk is assumed to be managed by active collision prediction and avoidance. Cost was measured in terms of maneuver frequency. The analysis was performed on a hypothetical satellite constellation. The results of the study indicate that the cost of collision risk management is very sensitive to orbit data quality. Significant collision risk reduction is shown to be very expensive using orbit data of low accuracy. If low-Earth-orbit optical tracker technology can be developed that can produce orbit accuracies similar to those of the Raven telescope in geosynchronous orbit, then significant collision risk reduction may be feasible.

Nomenclature

A_{ep}	=	area in encounter plane, km^2
C_p	=	3×3 position error covariance matrix, km^2
e	=	orbital eccentricity
$f(r_e)$	=	position error probability density function, 1/km^3
N_{ca}	=	number of close approaches
p_C	=	collision probability at conjunction averaged over approach direction
R_{cc}	=	radius of the collision cross section, km
r	=	radial miss distance, km
r_e	=	position error vector, km
T_{tf}	=	mission time frame, s
t_{age}	=	age of orbital data, days
u, v	=	intermediate variables in Chan's formulation[11]
v_{rel}	=	average relative velocity, km/s
ρ	=	spatial number density of objects, number/km^3
σ_{ch}	=	combined equivalent circular probability density function (PDF) standard deviation in the horizontal plane, km
σ_{cp}	=	equivalent circular PDF standard deviation for the primary object, km
σ_{cr}	=	combined one-sigma ellipsoid principal semiaxis in the radial direction, km
σ_{cs}	=	equivalent circular PDF standard deviation for the secondary object, km
σ_e	=	standard deviation of equivalent circular probability density function, km
σ_{np}	=	one-sigma ellipsoid principal semiaxis in the orbit-normal direction for the primary object, km
σ_{ns}	=	one-sigma ellipsoid principal semiaxis in the orbit-normal direction for the secondary object, km
σ_{rp}	=	one-sigma ellipsoid principal semiaxis in the radial direction for the primary object, km
σ_{rs}	=	one-sigma ellipsoid principal semiaxis in the radial direction for the secondary object, km
σ_{tp}	=	one-sigma ellipsoid principal semiaxis in the transverse direction for the primary object, km
σ_{ts}	=	one-sigma ellipsoid principal semiaxis in the transverse direction for the secondary object, km
σ_x	=	standard deviation of position error in encounter frame x direction, km
σ_z	=	standard deviation of position error in encounter frame z direction, km
$\sigma_1, \sigma_2, \sigma_3$	=	one-sigma ellipsoid principal semiaxes, km
$3\sigma_n$	=	three-sigma ellipsoid principal semiaxis in the orbit-normal direction, km
$3\sigma_r$	=	three-sigma ellipsoid principal semiaxis in the radial direction, km
$3\sigma_t$	=	three-sigma ellipsoid principal semiaxis in the transverse direction, km

Presented as Paper 2002-1810 at the AIAA SatMax 2002 Satellite Performance Workshop, Arlington, VA, 22 April 2002; received 14 January 2003; revision received 8 July 2003; accepted for publication 11 August 2003.

*Senior Engineering Specialist, Astrodynamics Department, P.O. Box 92957; Alan.B.Jenkin@aero.org. Senior Member AIAA.

Introduction

COLLISION risk management is an emerging issue in the operation of satellites. Several low Earth orbit (LEO) and geosynchronous (GEO) constellations have begun monitoring close approaches on a regular basis. Collision prediction services for INTELSAT were previously provided by The Aerospace Corporation for several years.[1] Motorola also received similar services from Aerospace for the Iridium constellation while it was the system operator. Several commercial GEO operators have received collision prediction services from the Massachusetts Institute of Technology/Lincoln Laboratory.[2] NASA manned programs, that is, the space shuttle and International Space Station (ISS), receive collision monitoring analysis support from U.S. Space Command and have performed maneuvers on multiple occasions.[3] The first verified natural collision occurred in 1996 between the operational satellite Cerise and a fragment from an Ariane upper stage that exploded in 1986.[4,5]

The primary obstacle to performing effective collision prediction has been the lack of access to accurate orbit data on threat objects. Accurate orbital data are generally available on primary objects, that is, operational satellites, because the operators perform orbit determination based on active cooperative ranging (via radio frequency link or laser) and also have knowledge of planned maneuvers. However, for close approaches between active satellites, operators of the two satellites are often reluctant to share orbital ephemerides. If the secondary object is inactive or debris, then the only orbital data historically available to the broad space sector are U.S. Space Command two-line element sets (TLEs). Several independent studies have shown that TLEs generally have position errors on the order of kilometers.[6–9] NASA has circumvented this problem via a special arrangement with U.S. Space Command, whereby it receives higher accuracy special perturbations (SP) vectors for identified shuttle and ISS conjunctions.[3] In general, however, SP data are not available to the broad space sector.

Orbit data quality affects several important operational issues that arise in collision risk management. One such issue is operator reaction time. Enough time must be available between the decision to

maneuver and the predicted conjunction to perform the required maneuver analysis and operational procedures. If error growth is large during this period, then a greater maneuver effort will be required to reduce collision risk to a desired level than would be required if the error growth were small. This issue was studied by Gottlieb et al. for a constellation of LEO satellites that have constraints on collision avoidance maneuvers.[7]

Another issue affected by orbit data quality is the frequency of maneuvers and the associated impact on operational workload and satellite system performance or revenue generation due to outages. A study of the relationship between collision risk reduction and maneuver frequency for the ISS was performed by Foster.[3] The ISS is a very large vehicle, and a high frequency of maneuvers would be very costly in terms of propellant. It would also be very disruptive to the microgravity science mission because long periods of time are required for maneuver-induced structural disturbances to dampen. In spite of the large size of the ISS, Foster showed that it was possible to reduce collision risk by approximately a factor of five below the latent risk of 10^{-3} per year with two maneuvers per year, on average. This result is made possible by two factors. First, the ISS operates in a LEO orbital regime of relatively low population density. Second, ISS collision avoidance uses SP orbital data for the secondary threat objects. These data are more accurate than TLEs because they are generated using direct numerical integration of a force model, whereas TLEs are generated using an analytical mean element theory. This work was performed by Foster[3] and Foster and Estes[10] from the early to late 1990s.

Similar but completely independent studies have been performed by the author since late 1999 for several LEO and GEO constellations. Although these constellations consist of satellites that are much smaller than the ISS, they contain multiple satellites and typically operate in regimes of relatively high population density. In addition, commercial systems have historically only had access to TLEs. As a result, the risk vs cost tradeoff is considerably less favorable than for the ISS.

This paper presents a quantitative analysis of the effect of orbit data quality on the cost of collision risk management for LEO constellations. The variation of maneuver frequency and achievable levels of risk reduction with different classes of orbit data is discussed.

Collision Probability at Conjunction

Collision probability at conjunction depends on errors in the knowledge of the positions of the conjuncting objects. Orbit data position error r_e is typically modeled as a random vector variable with a three-dimensional Gaussian probability density function (PDF) $f(r_e)$:

$$f(r_e) = \left[1\Big/\sqrt{(2\pi)^3|C_p|}\right]\exp\left(-\left[\tfrac{1}{2}r_e^T C_p^{-1} r_e\right]\right) \qquad (1)$$

where C_p is the 3×3 position submatrix of the 6×6 state error covariance matrix. An ellipsoid surface of constant probability density centered on the primary and secondary objects is determined by setting the argument of the exponential function in Eq. (1) equal to a constant. Ellipsoid surfaces can, therefore, be determined from the associated covariance matrix C_p for each object. The principal semiaxes of the so-called three-sigma ellipsoid are obtained from C_p by diagonalization:

$$C_{pd} = M^{-1}C_p M = \begin{bmatrix} \sigma_1^2 & 0 & 0 \\ 0 & \sigma_2^2 & 0 \\ 0 & 0 & \sigma_3^2 \end{bmatrix} \qquad (2)$$

where M is the modal matrix of C_p. The three-sigma principle semiaxes are then $3\sigma_1$, $3\sigma_2$, and $3\sigma_3$.

As the orbit data become less accurate, the probability mass under the PDF surface (which must always sum to unity) is spread out over larger distances, and the corresponding three-sigma ellipsoid becomes larger. The three-sigma position error ellipsoids are shown in Fig. 1.

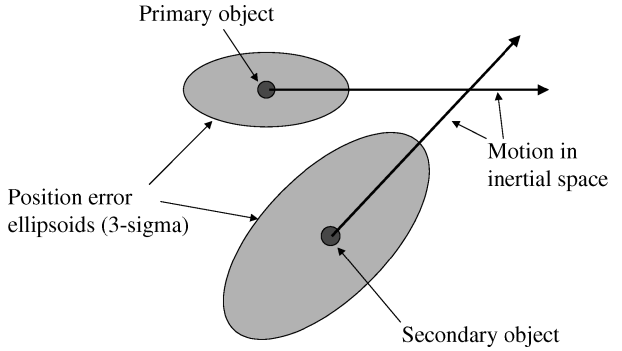

Fig. 1 Two objects near conjunction along with position error ellipsoids (three sigma).

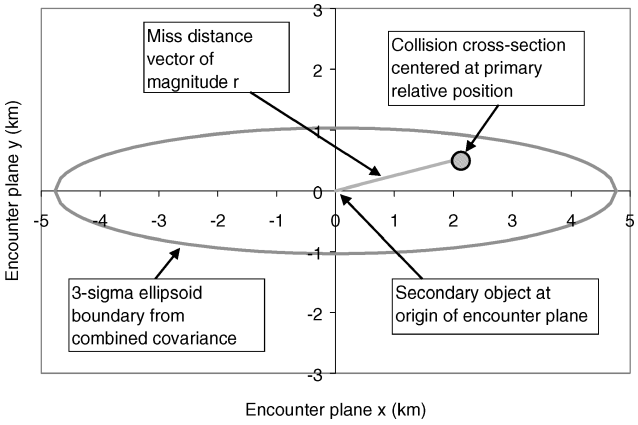

Fig. 2 Encounter plane with three-sigma error ellipse centered at the secondary object.

Collision probability for a given conjunction is generally analyzed by considering the relative geometry between the primary and secondary vehicles in the encounter plane.[10–13] Figure 2 shows one choice of the encounter plane whereby the origin is placed at the center of the secondary object. The z axis, which emanates from Fig. 2, points in the direction that is opposite to the direction of the relative velocity vector of the primary with respect to the secondary at time of conjunction. The error statistics of the two objects are typically represented by a single ellipse centered on the secondary object. This ellipse is obtained by adding the covariance matrices of the two objects (in a common coordinate system, such as Earth centered inertial) and then projecting the corresponding ellipsoid onto the encounter plane. The coordinate frame is then rotated about the z axis so that the x axis points along the major axis of the ellipse.

Given the predicted relative distance vector at conjunction, a three-sigma error ellipse in the encounter plane, and a collision cross-section centered at the primary, it is then possible to compute the collision probability using any one of several formulations.[10–13] This procedure is justified as long as the position errors of the two objects are statistically independent and the relative velocity during conjunction is high enough so that the three-dimensional ellipsoids of the two objects change insignificantly while they overlap. These conditions hold for most noncoplanar encounters in LEO.

If the computed collision probability exceeds a given threshold, then an action may be taken to reduce the risk. If more accurate orbital data cannot be obtained, a maneuver is necessary to reduce the risk. Clearly, the frequency of these maneuvers is dependent on the frequency of close approaches and the distribution of the size of the combined projected ellipse, that is, the quality of the orbit data.

Close Approach Frequency

The frequency of close approaches as a function of miss distance can be determined from the distribution of miss distance over the mission timeframe. To generate a sample miss distance distribution,

a hypothetical LEO satellite constellation was considered. This constellation consists of 40 satellites with a mean altitude of 850 km and a shell width (apogee–perigee spread) of 10 km. The constellation satellites all have an orbital inclination of 64 deg. There are eight planes spread out uniformly in right ascension, with five satellites in each plane.

The preferred method to generate the miss distance distribution is to simulate directly the orbital motion of the constellation primaries and the threat secondaries in the background population and compute all of the conjunctions and miss distances over the mission time frame. Whereas this would in general be performed for a specific constellation, it is more expedient for the hypothetical constellation, considering that it exists for illustration purposes only, to perform an approximate analysis using a density-based method.

Similar to the kinetic theory of molecular gases, the density-based method considers threat objects to be randomly and independently distributed within a given volume of space. The following simple formulation can then be used:

$$N_{\text{ca}} = \rho v_{\text{rel}} A_{\text{ep}} T_{\text{tf}} \tag{3}$$

where N_{ca} is the number of close approaches that occur during the mission time frame T_{tf}, ρ is the threat object spatial number density, v_{rel} is the relative velocity magnitude between primary object and threat object averaged over the mission time frame and all of the threat objects in the local field, and A_{ep} is the area in the encounter plane centered at the primary object.

The usual approach for computing spatial density is to assume that the threat objects are individually distributed throughout toroidal volumes. This is justified as long as the orbital motion over the time frame of interest is dominated by the perturbation induced by the J_2 zonal harmonic of the Earth's gravity field and the orbits undergo many complete apsidal and nodal rotations. For this study, the density ρ was computed by D. L Mains of The Aerospace Corporation using the computer program DENSITY to process the unclassified U.S. Space Command catalog of resident space objects dated 4 March 1999. This tool uses the formulation derived by Dennis,[14] which is equivalent to that of Kessler.[15]

The average encounter velocity v_{rel} was estimated to be 9.46 km/s. The mission time frame T_{tf} was assumed to be 10 years. The encounter plane area A_{ep} is equal to πr^2, where r is the miss distance at close approach. The resulting average number of close approaches as a function of area radius r is shown in Fig. 3. This curve is the cumulative distribution of miss distances over the mission time frame for the hypothetical constellation.

Based on a comparison study in Ref. 16, this density-based distribution is estimated to be accurate to within 50% on average relative to the distribution that would be generated by a detailed conjunction simulation. This level of accuracy is reasonable given the general uncertainties that are involved in computing long-term collision probability, such as uncertainties in long-term propagation and size estimation of background objects.

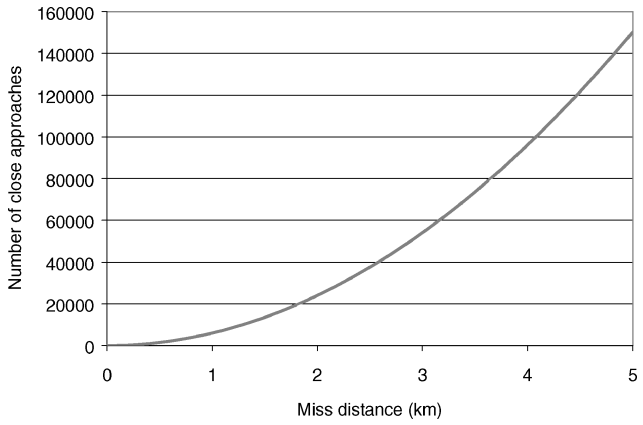

Fig. 3 Cumulative distribution of close approach miss distances over mission time frame for the hypothetical LEO constellation.

Orbit Data Error Models

To understand typical conjunction scenarios, it is useful to obtain an estimate of the average encounter plane ellipse dimensions. For primary and secondary objects that move on orbits with low eccentricity, that is, $e < 0.2$, the long axis of the ellipsoids will be mostly confined to the local horizontal plane, as will the relative velocity vector of the primary referenced to the secondary. This geometry is shown in Fig. 4, which shows the encounter in the z–x components of the encounter frame. The perspective is from the positive y axis looking toward the negative direction. Because threat objects have orbits with a wide range of inclinations, the orientation of the long axis of the ellipsoid can vary within the z–x plane over 360 deg. The line segment along the x axis represents the x component of the average projection of the ellipsoids onto the encounter plane that results if the ellipsoid orientation is randomly and uniformly distributed over 360 deg.

The ellipsoid dimensions in Fig. 4 represent an average close approach scenario between a primary object in the hypothetical constellation and a secondary object from the trackable background population and were determined from models of the primary and secondary object position errors. It was assumed that primary object orbit data are computed from dedicated ranging. The following position error model was used for the primary object, it is a modification of one employed in Ref. 7 for cooperatively ranged LEO satellites:

$$3\sigma_t = 0.03 + 0.193 t_{\text{age}} \tag{4}$$

$$3\sigma_n = 0.03 + 0.2 \times 0.193 t_{\text{age}} \tag{5}$$

$$3\sigma_r = 0.03 + 0.1 \times 0.193 t_{\text{age}} \tag{6}$$

where $3\sigma_t$, $3\sigma_n$, and $3\sigma_r$ are the transverse, normal, and radial semiaxes of the three-sigma ellipsoid in kilometers and t_{age} is the age, in days, of the orbit data at predicted conjunction referenced to the epoch date associated with the data. It was assumed that data age is uniformly distributed between 0.125 and 1.0 days. The age bounds are based on the assumption that an orbit update can be obtained once per day and that the latest it would be available is 3 h before conjunction.

The dimensions of the three-sigma error ellipsoid for a typical secondary object were generated using the following model:

$$3\sigma_t = 3.6 + 2.27 t_{\text{age}} + 0.51 t_{\text{age}}^2 \tag{7}$$

$$3\sigma_n = 1.12 + 0.12 t_{\text{age}} \tag{8}$$

$$3\sigma_r = 0.6 + 0.11 t_{\text{age}} + 0.01 t_{\text{age}}^2 \tag{9}$$

This particular model was obtained by averaging error models for a set of LEO objects determined using the algorithm described in

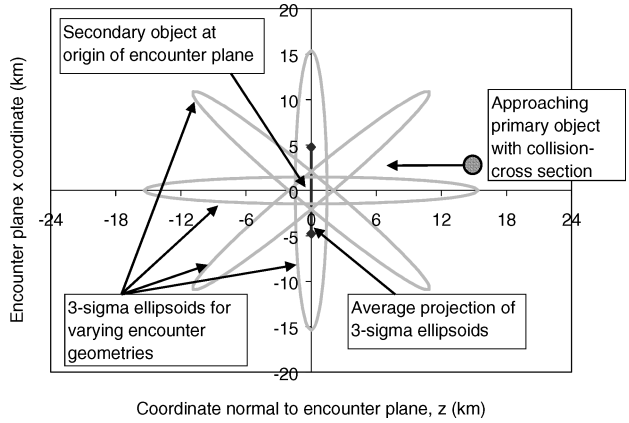

Fig. 4 Possible orientations of the error ellipsoid long axis in z–x encounter frame coordinates and corresponding average projection onto the encounter plane.

Ref. 6. Therefore, it is an average representation of orbit data that were publicly available during the study in Ref. 6. In the present study, it was assumed that data age is uniformly distributed between 0.857 and 5.284 days. The age bounds include the assumption that a predicted conjunction occurs at most one day after the data are obtained.

Note that these error models predict the average secular evolution of the error ellipsoid and do not include the oscillation due to orbital periodicity. When error models that include this oscillation become available, it is recommended that they be included when considering specific satellite constellations.

From these error models, it is seen that the secondary object ellipsoid is much larger than the primary object ellipsoid and completely dominates the combined ellipsoid. The resulting time-averaged three-sigma principal semiaxes were 15.4 and 1.47 km in the z–x plane and 1.03 km along the y axis. The average projection on the x axis is approximately 4.76 km. These ellipsoids are those shown in Fig. 4.

Combined Effect of Errors and Close Approach Frequency

The average projection of the combined ellipsoid onto the encounter plane is shown in Fig. 5. This ellipse is labeled lower accuracy data in Fig. 5. Overlaid on this ellipse are contours of constant cumulative number of close approaches over the mission. The number by each contour shows the average expected number of penetrations of the encounter plane within the circle indicated by the contour. It can be seen that the ellipse overlaps many contours corresponding to tens of thousands of close approaches.

Let us suppose that it is possible to obtain orbit data that are three times more accurate. In other words, the secondary object errors are also modeled by Eqs. (7–9), but then are divided by 3. Such an improvement in accuracy might be obtained by more frequent sensor tasking and data refreshment, thereby decreasing data age, or by more accurate orbit determination and propagation. The ellipse corresponding to this higher accuracy data is also shown in Fig. 5. It can be seen that this ellipse overlaps contours corresponding to many fewer close approaches, more on the order of thousands rather than tens of thousands. This implies that a given reduction in orbit data error can lead to a proportionately greater reduction in maneuver frequency.

Suppose that maneuver constraints permit an increase in the predicted miss distance along a straight line as shown in Fig. 5. For a given satellite, it is possible to determine the reduction in collision probability at conjunction as a function of increasing miss distance along the line, and this is illustrated in Fig. 6. In this case, the line was selected to yield the average case, assuming that the slope angle of the miss distance vector in the encounter plane for all of the close approaches is randomly and uniformly distributed over 360 deg. The collision probability was computed by multiplying the PDF in the encounter plane by the average collision cross section A_{cc} between

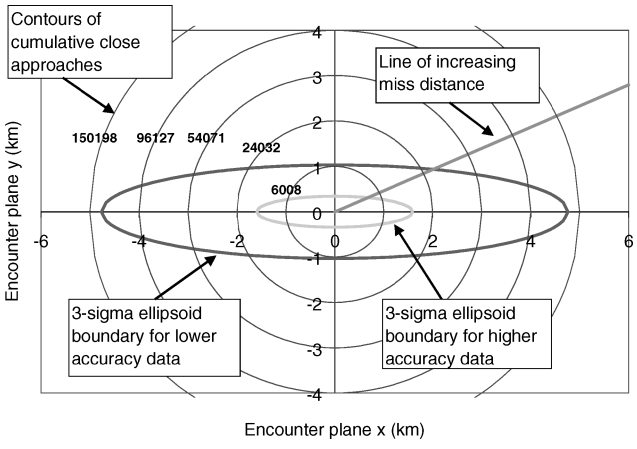

Fig. 5 Average error ellipses in the encounter plane and contours of constant cumulative close approaches over the mission.

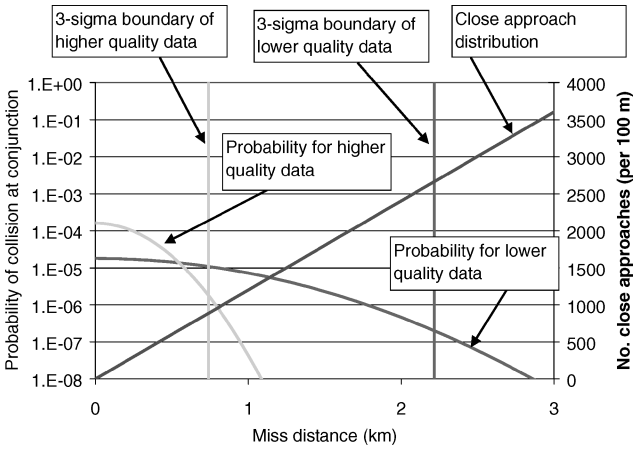

Fig. 6 Collision probability and frequency of close approaches, both as functions of miss distance.

the primary object and secondary objects in the background. This procedure is valid as long as the PDFs vary little over A_{cc}. This constraint is satisfied in this case because the collision cross section A_{cc} was assumed to be circular with a radius of 4.44 m, which is much smaller than the dimensions of the encounter plane ellipse. This keepout radius approximately yields the average collision cross section that resulted by considering all pairings of a primary spacecraft of diameter 7 m with all LEO background objects listed in the unclassified U.S. Space Command catalog.

The collision probability for both the lower quality and higher quality data is shown in Fig. 6. The miss distances that cross the three-sigma ellipses of Fig. 5 are also shown for both data categories. In addition, the differential distribution of miss distance is overlaid. This distribution is effectively a histogram, which shows the number of close approaches over the mission within 100-m miss distance bins, and is obtained by computing finite differences from the curve in Fig. 3. In essence, Fig. 6 shows relative frequency of occurrences of different values of conjunction miss distance and the average corresponding collision probability for each miss distance and data type.

From Fig. 6, it is possible to note an important effect of decreasing orbit data accuracy. At smaller miss distances, where there are fewer conjunctions, the probability of collision is lower for the data of lower quality than for the data of higher quality. However, at larger miss distances, where there are more conjunctions, the probability of collision is actually higher for the data of lower quality than for the data of higher quality. This result occurs because as orbit data quality decreases, the probability mass under the PDF is squeezed out from smaller to larger miss distances. Therefore, decreasing data quality actually increases collision probability at larger distances.

It is possible to quantify the frequency of occurrence of various levels of collision probability. This quantification was accomplished as follows. First, the error ellipsoid distributions for both the primary and secondary objects were determined from the models of Eqs. (4–6) and (7–9) and the assumption of uniformly distributed data ages. Next, collision probabilities were computed for combinations of a wide range of miss distances and error ellipsoids. Each collision probability was assigned a statistical weight determined by 1) the error ellipsoid distribution for each given error ellipsoid and 2) the differential miss distance distribution of Fig. 6 for the given miss distance. The statistical weights of the collision probabilities were deposited in histogram bins. This process was essentially implemented as a three-dimensional numerical convolution integration.

For this computation, the miss distance vector was assumed to be restricted to the vertical plane, and its orientation within the vertical plane was assumed to be randomly and uniformly distributed over 360 deg. These assumptions are approximate but motivated the use of Chan's formulation of collision probability based on equivalent circles[11] to approximate rapidly the average collision probability, thereby avoiding the dramatic increase in the computational effort that would be associated with a direct sweep of all encounter

directions and primary/secondary ellipsoid combinations. Chan showed that, when the error ellipse has random orientation in the encounter plane, the average PDF of the position error can be approximated by an equivalent circular PDF with standard deviation equal to the geometric mean of the one-sigma ellipse principal semiaxes:

$$\sigma_e = \sqrt{\sigma_x \sigma_z} \tag{10}$$

The average collision probability can then be approximated by the following formula:

$$p_C = \exp[-(v/2)]\{1 - \exp[-(u/2)]\} \tag{11}$$

where $u = (R_{cc}/\sigma_e)^2$ and $v = (r/\sigma_e)^2$. R_{cc} is the radius of the collision cross-section (in this case 4.44 m), and r is the miss distance.

For this study, the value of σ_e was computed as follows. It was assumed that the primary object and the majority of secondary objects move on orbits of low eccentricity. Hence, the long axes of the error ellipsoids of both objects are mostly constrained to the local horizontal plane. In addition, it was assumed that secondary object orbits have a wide variety of inclinations. Therefore, over many encounters the orientations of the primary and secondary object ellipsoids in the horizontal plane appear random in the encounter frame. The equivalent circle radii in the horizontal plane for both objects are then

$$\sigma_{cp} = \sqrt{\sigma_{tp}\sigma_{np}} \tag{12}$$

$$\sigma_{cs} = \sqrt{\sigma_{ts}\sigma_{ns}} \tag{13}$$

where the subscript p designates the primary object, s the secondary object, t the transverse direction, n the orbit normal direction, and c the equivalent circle. Because the primary and secondary errors are statistically independent, the combined circle radius in the horizontal plane is

$$\sigma_{ch} = \sqrt{\sigma_{cp}^2 + \sigma_{cs}^2} \tag{14}$$

where the subscript h designates the horizontal plane. This quantity represents the average projection of the horizontal-plane principal semiaxes of the combined error ellipsoid into the encounter frame.

Because it is assumed that most objects reside on orbits of low eccentricity, the relative velocity between both objects has a small radial component, and the radial principal semiaxes of the error ellipsoids can be assumed to translate directly into the encounter frame. The combined radial standard deviation is then

$$\sigma_{cr} = \sqrt{\sigma_{rp}^2 + \sigma_{rs}^2} \tag{15}$$

where the subscript r designates the orbit radial direction.

The miss distance vector is mostly confined to the vertical plane due to the assumption of low orbit eccentricity. However, it can have a wide variety of orientations within that plane. If the encounter frame is always rotated so that the miss distance vector is aligned along the x axis, then the orientation of the error ellipse over many encounters will appear random relative to the primary. Hence, the horizontal and radial standard deviations can be used to compute the equivalent circle standard deviation in the encounter frame:

$$\sigma_e = \sqrt{\sigma_{ch}\sigma_{cr}} \tag{16}$$

The procedure generated the histograms of predicted collision probabilities shown in Figs. 7 and 8. As can be seen, the quantitative analysis verifies that, as data quality decreases, the maximum collision probability at conjunction decreases, but the number of conjunctions at lower collision probabilities increases dramatically.

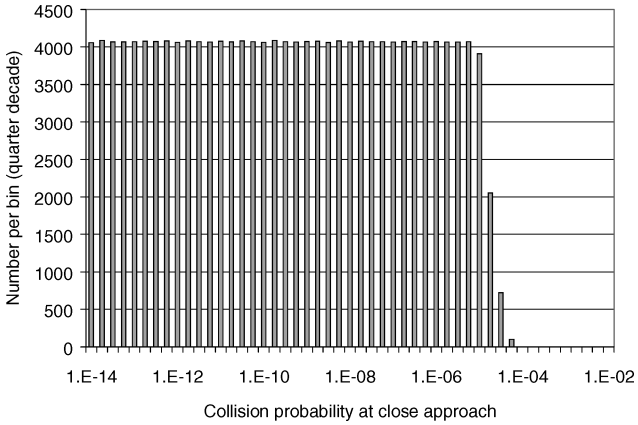

Fig. 7 Histogram of predicted collision probability at conjunction for the hypothetical constellation and lower quality secondary object data (bin width equal to one-quarter decade).

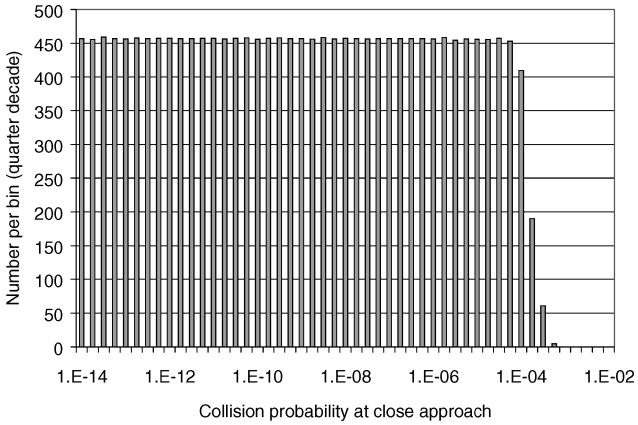

Fig. 8 Histogram of predicted collision probability at conjunction for the hypothetical constellation and higher quality secondary object data (bin width equal to one-quarter decade).

Maneuver Frequency and the χ Plot

Assuming that collision avoidance maneuvers are triggered whenever predicted collision probability at conjunction exceeds a threshold, the maneuver frequency can then be determined from the histograms of predicted collision probability in Figs. 7 and 8. For each threshold value, the number of maneuvers is computed by summing over the collision probability histogram from the threshold up to the maximum possible value of unity.

To determine the threshold, it is necessary to relate it to the desired reduction in total collision risk over mission. The total risk of collision over the mission is obtained by combining the collision probabilities at each conjunction assuming that the orbit data errors at different conjunction are statistically independent. To minimize the impact of the maneuver on operations, it is assumed that conjunction collision probabilities that exceed the threshold will be reduced to the threshold and no lower. In the collision probability histogram, all occurrences at probabilities above the threshold are then shifted down to the threshold itself. This conservation of collision probability is necessary to prevent underestimating the amount of total risk that will actually remain after the maneuvers are performed.

From this procedure, it is possible to construct a graphical analysis tool called the χ *plot*. This plot, illustrated in Fig. 9, contains two overlaid curves. The monotonically decreasing curve shows maneuver frequency per year vs conjunction collision probability threshold. The monotonically rising curve shows total collision risk over mission vs threshold. The χ plot effectively shows how to select a threshold to achieve a given desired amount of total risk over mission and how much it will cost in terms of maneuver frequency. The designation comes from the observation that the two curves together generally form a wavy X, or Greek letter χ.

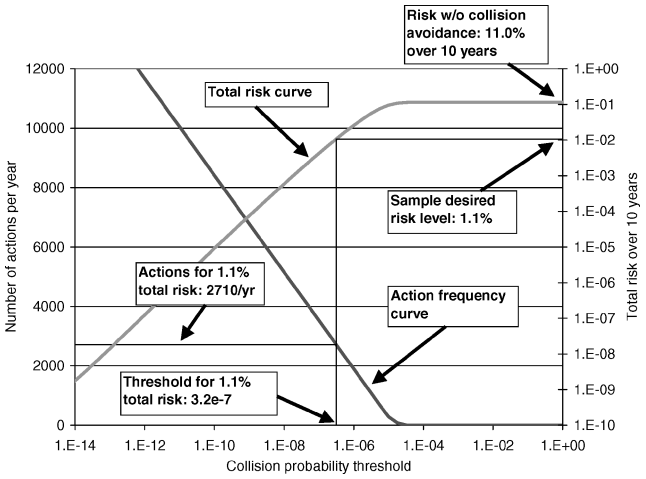

Fig. 9 Hypothetical constellation χ plot with lower quality secondary object data.

Figure 9 shows the resulting χ plot generated from the collision probability distribution in Fig. 7. It applies to the hypothetical constellation used in this study and assumes that the secondary threat objects have orbital data errors described by Eqs. (7–9) that is, the lower quality data. The right side of the total risk curve is flat because collision probability thresholds in this region are so high that they are never violated, as shown by the action frequency curve. Hence, local changes in threshold have no effect on total collision risk. This result is directly attributable to the orbit data quality. The total latent risk of collision for the entire constellation over the 10-year mission is represented by the flat portion of the total risk curve and is approximately 11%. In other words, the odds that any member of the constellation will collide with a background object are approximately 11 in 100. The corresponding collision risk posed to each individual satellite is 0.275%. If it is desired to reduce the total risk by a factor of 10, then from the sloped region of the total risk curve, it is seen that a collision probability threshold for individual conjunctions of 3.2×10^{-7} must be selected. From the maneuver frequency curve, it is seen that this threshold will then be exceeded 2710 times each year on average for the entire constellation. Each individual satellite will experience an average maneuver rate of 68 per year. Such a high threshold violation frequency is attributable to the fact that the background population density is very high at the 850-km altitude and that the constellation contains many satellites (40), thereby resulting in many penetrations of the large combined error ellipse in the encounter plane each year.

A maneuver rate of 2710 times per year is unmanageable, and therefore, it is not feasible to achieve a reduction in total mission collision risk by an order of magnitude. At a more reasonable maneuver rate of one per month, the achievable reduction in collision risk is negligible. This result demonstrates that, for the hypothetical constellation used in this study, it is very expensive to achieve significant collision risk reduction using orbit data of low accuracy.

The quantitative results of this analysis are approximate due to the assumptions embedded in the formulation of the collision probability averaged over encounter geometry. When considering a specific satellite constellation, it is recommended that a detailed conjunction simulation that computes miss distance vectors and collision probability at each conjunction be used to generate these histograms. In Ref. 17, a recent study by the author and a colleague is presented that used a detailed conjunction simulation for geosynchronous satellites to assess the impact of data quality on the feasibility of collision risk management. Figures 5 and 6 in Ref. 17 show that a maneuver frequency of approximately 200 per year is required to achieve a reduction in collision risk by a factor of 10 for the publicly available data that were used. The maneuver frequency in that study is lower than in the current study because the latent geosynchronous collision risk computed in that study of 0.0016 is almost two orders of magnitude lower than the latent risk of 0.11 for the hypothetical LEO constellation considered in this study. Because maneuver frequency should roughly scale with latent collision probability, that is, collision frequency, when the risk reduction factor is held constant, it would be expected that maneuver frequency in the current study would be higher by one to two orders of magnitude. The maneuver frequency that resulted in this study of 2710 per year is in fact a little more than an order of magnitude larger than the frequency of 200 per year. Therefore, the approximate maneuver frequency of 2710 per year is within the expected range and may possibly be a low estimate. Therefore, it is clear that low data quality induces high maneuver frequencies for reasonable amounts of collision risk reduction.

Cost vs Data Quality

When χ-plot analysis is used, it is possible to quantify the cost of collision risk management, measured in terms of yearly maneuvers, as a function of secondary object orbit data quality. For the hypothetical constellation used in this analysis, Fig. 10 shows yearly maneuver frequency as a function of desired total collision risk over mission for several levels of data quality. The curve labeled lower accuracy data corresponds to the error model of Eqs. (7–9).

The curve labeled higher accuracy data corresponds to data that are three times more accurate. Again, such data might be obtained by increasing the orbit data refreshment rate or by improving the orbit determination process. Note that, as the number of maneuvers is reduced to zero, the two curves converge to the same latent total risk, accounting for some slight difference caused by numerical roundoff. The latent total risk is invariant with data quality as long as there is no correlation amongst the object positions that is masked by the errors of the lower quality data but would be evident in the higher quality data. It is seen from Fig. 10 that, even with the higher accuracy data, 310 maneuvers per year for the entire constellation are still required to reduce total collision risk by a factor of 10. This translates to an average maneuver rate of seven to eight times per year for each individual satellite. Although this maneuver frequency is a dramatic improvement, it is still very expensive.

Another potential option for obtaining orbit data on secondary threat objects is to use dedicated portable optical trackers. Examples of such technologies are The Boeing Company T-Tracker[18] and the Raven telescope.[19–22] Although the author is not currently aware that high-accuracy orbit determination has been performed for LEO objects using portable optical trackers, high accuracy for GEO and semisynchronous orbits has been demonstrated with the Raven. To obtain an idea of the improvement that might be obtained if Raven-type accuracy were available for LEO objects, a χ-plot analysis was performed for the study constellation assuming a Raven-like error model for the secondary object orbit data:

$$3\sigma_t = 0.375 + 0.225 t_{\text{age}} \tag{17}$$

$$3\sigma_n = 0.088 + 0.0529 t_{\text{age}} \tag{18}$$

$$3\sigma_r = 0.0806 + 0.0484 t_{\text{age}} \tag{19}$$

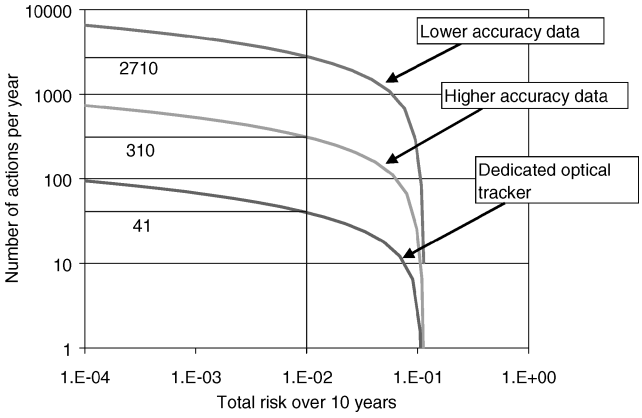

Fig. 10 Cost, in terms of maneuver frequency, of collision risk management for three different types of secondary object data quality.

The data age was uniformly distributed between 1 and 3 days. This condition assumes that the earliest that an orbit determination might be performed and completed would be 3 days before predicted conjunction and that the latest would be 1 day before conjunction. Clearly, this is a crude extrapolation of GEO-like performance to LEO with some additional accounting for larger normal and radial error growth rates due to atmospheric drag influences. A more detailed determination of the error model for a LEO optical tracker would be necessary before the last word could be said about the benefits to collision risk management. For this study, the model is used to give a glimpse of what might be achievable.

The resulting curve for secondary object orbit data from a dedicated optical tracker, shown in Fig. 10, indicates that it might be possible to reduce total mission risk for the hypothetical constellation by a factor of 10 with only 41 maneuvers per year for the entire constellation. This frequency equates to approximately three to four maneuvers per month, or one maneuver per year for each individual satellite. This maneuver frequency is operationally much more manageable than appears to be possible using the earlier two data types.

Conclusions

An analysis was performed to determine the effect of orbit data quality on the feasibility of performing collision risk management. A hypothetical LEO constellation was used for this analysis. As part of this work, an analysis tool called the χ plot was developed. This tool permits selection of conjunction collision probability thresholds required to attain desired levels of total risk reduction over a mission and indicates the associated cost in terms of maneuver frequency. The results of the study indicate that the cost of collision risk management, measured in terms of maneuver frequency, is very high when orbit data of low accuracy are used. This conclusion is generally applicable to orbital systems with significant total collision risk over mission time frame, such as constellations, space stations, and tethers that operate in highly populated orbital regions. If LEO optical tracker technology can be developed that can produce orbit accuracies similar to those of the Raven telescope in GEO, then the cost of collision risk management for these systems can be significantly reduced.

Acknowledgments

Internal support for this work was provided by the Center for Orbital and Reentry Debris Studies (CORDS). The author thanks several individuals at The Aerospace Corporation for their assistance in preparing this paper. Technical committee members G. E. Peterson, E. T. Campbell, and W. H. Ailor (Director, CORDS) provided technical review of the paper. B. J. Steppe provided publication review.

References

[1]Oltrogge, D., Gist, R. G., Raman, K., and Chan, J., "Experiences with Situational Awareness for Communications Satellite Operations," AIAA Paper 2001-0075, April 2001.

[2]LeClair, R. A., and Sridharan, R., "Probability of Collision in the Geostationary Orbit," *Proceedings of the Third European Conference on Space Debris*, edited by H. Sawaya-Lacoste, ESA SP-473, Vol. 1, 2001, pp. 463–470.

[3]Foster, J.L., Jr., "The Analytical Basis for Debris Avoidance Operations for the International Space Station," *Proceedings of the Third European Conference on Space Debris*, edited by H. Sawaya-Lacoste, ESA SP-473, Vol. 1, 2001, pp. 441–445.

[4]Alby, F., Lansard, E., and Michal, T., "Collision of Cerise with Space Debris," *Proceedings of the Second European Conference on Space Debris*, edited by B. Kaldeich-Schürmann and R. Harris, ESA SP-393, 1997, pp. 589–596.

[5]Payne, T. P., "First 'Confirmed' Natural Collision Between Two Cataloged Satellites," *Proceedings of the Second European Conference on Space Debris*, edited by B. Kaldeich-Schürmann and R. Harris, ESA SP-393, 1997, pp. 597–600.

[6]Peterson, G. E., Gist, R. G., and Oltrogge, D. L., "Covariance Generation for Space Objects Using Public Data," *Advances in the Astronautical Sciences*, Vol. 108, Feb. 2001, pp. 201–214.

[7]Gottlieb, R. G., Sponaugle, S. J., and Gaylor, D. E., "Orbit Determination Accuracy Requirements for Collision Avoidance," *Advances in the Astronautical Sciences*, Vol. 108, Feb. 2001, pp. 1105–1122.

[8]Chan, J. C., and Navarro, D., "Comparisons of NORAD Two-Line Elements with Intelsat Data Orbital Elements," *Proceedings of the Third European Conference on Space Debris*, edited by H. Sawaya-Lacoste, ESA SP-473, Vol. 2, 2001, pp. 771–779.

[9]Deguine, B., Foliard, J., and Alby, F., "Covariance Modeling in Satellite Collision Risk Activities," AIAA Paper 2002-4631, Aug. 2002.

[10]Foster, J. L., and Estes, H. S., "A Parametric Analysis of Orbital Debris Collision Probability and Maneuver Rate for Space Vehicles," NASA JSC 25898, Aug. 1992.

[11]Chan, K. F., "Collision Probability Analyses for Earth Orbiting Satellites," *Advances in the Astronautical Sciences*, Vol. 96, Nov. 1997, pp. 1033–1048.

[12]Chobotov, V. A., "The Collision Hazard in Space," *Journal of the Astronautical Sciences*, Vol. 30, No. 3, 1982, pp. 191–212.

[13]Patera, R. P., "General Method for Calculating Satellite Collision Probability," *Journal of Guidance, Control, and Dynamics*, Vol. 24, No. 4, 2001, pp. 716–722.

[14]Dennis, N. G., "Probabilistic Theory and Statistical Distribution of Earth Satellites," *Journal of the British Interplanetary Society*, Vol. 25, 1972, pp. 333–376.

[15]Kessler, D. J., "Derivation of the Collision Probability between Orbiting Objects: The Lifetimes of Jupiter's Outer Moons," *Icarus*, Vol. 48, 1981, pp. 39–48.

[16]Jenkin, A. B., and Gick, R. A., "Collision Risk Posed to the Global Positioning System by Disposal Orbit Instability," *Journal of Spacecraft and Rockets*, Vol. 39, No. 4, 2002, pp. 532–539.

[17]Jenkin, A. B., and Peterson, G. E., "Collision Risk Management in Geosynchronous Orbit," Committee on Space Research, Rept. PEDAS1-B1.4-0049-02, 34th COSPAR Scientific Assembly, Elsevier, Orlando, FL, Oct. 2002.

[18]Tansey, R. J., Campbell, B., and Koumvakalis, A., "Description and Experimental Results of a 58lb Portable LEO Satellite Tracker," *Image Intensifiers and Applications; and Characteristics and Consequences of Space Debris and Near-Earth Objects*, edited by C. B. Johnson, T. D. Maclay, and F. A. Allahdadi, Proceedings of SPIE, Vol. 3434, Society of Photo-Optical Instrumentation Engineers, Bellingham, WA, 1998, pp. 78–87.

[19]Wallace, S., Sabol, C., and Carter, S., "Use of the Raven Optical Sensor for Deep Space Orbit Determination," *Advances in the Astronautical Sciences*, Vol. 97, Aug. 1997, pp. 1603–1624.

[20]Sabol, C., Burns, R., and Wallace, S., "Analysis of the Telstar-401/GOES-10 Close Approach Using the Raven Telescope," *Advances in the Astronautical Sciences*, Vol. 99, Feb. 1998, pp. 317–332.

[21]Chao, C. C., Cox, J., and Burns, R., "Ground Tracking and Control of GEO Cluster Satellites Using the Raven Telescope," *Advances in the Astronautical Sciences*, Vol. 108, Feb. 2001, pp. 901–912.

[22]Sabol, C., Luu, K. K., Kervin, P., Nishimoto, D., Hamada, K., and Sydney, P., "Recent Developments of the Raven Small Telescope Program," *Advances in the Astronautical Sciences*, Vol. 112, Feb. 2002, pp. 397–416.

N. Gatsonis
Associate Editor